Available online at www.sciencedirect.com
SCIENCE DIRECT
ELSEVIER
Journal of the European Ceramic Society 26 (2006) 2937–2943
ECERS
www.elsevier.com/locate/jeurceramsoc

Ferroelectric thin films obtained by pulsed laser deposition

A. Purice [a], G. Dinescu [a], N. Scarisoreanu [a], P. Verardi [b], F. Craciun [c], C. Galassi [d], M. Dinescu [a,*]

[a] National Institute for Laser, Plasma and Radiation Physics, P.O. Box MG–16, Magurele, 077125 Bucharest, Romania
[b] CNR-Istituto di Acustica, Via del Fosso del Cavaliere 100, I-00133 Rome, Italy
[c] CNR Istituto dei Sistemi Complessi, Area di Ricerca Tor Vergata, Via del Fosso del Cavaliere 100, I-00133 Roma, Italy
[d] CNR-ISTEC, Via Granarolo 64, I-48018 Faenza, Italy

Available online 4 May 2006

Abstract

We review our significant results concerning pulsed laser deposition (PLD) of some ferroelectric compounds: (i) lead magnesium niobate $Pb(Mg_{1/3}Nb_{2/3})O_3$ (PMN); (ii) lead magnesium niobate–lead titanate $Pb(Mg_{1/3}Nb_{2/3})O_3$–$PbTiO_3$ (PMN–PT), with variable PT contents; (iii) La-doped lead zirconate titanate $(Pb_{1-x}La_x)(Zr_{0.65}Ti_{0.33})O_3$ (PLZT); and (iv) Nb-doped lead zirconate titanate $Pb_{0.988}(Zr_{0.52}Ti_{0.48})_{0.976}Nb_{0.024}O_3$ (PNZT). A parametric study has been performed in order to evidence the influence of the deposition parameters (laser wavelength, laser fluence, oxygen pressure, substrate type and temperature, RF power discharge addition, etc.) on the film properties and to identify the best growing conditions. Techniques including atomic force microscopy (AFM), X-ray diffraction (XRD), scanning electron microscopy (SEM), secondary ions mass spectroscopy (SIMS), transmission electron microscopy (TEM), electrical and ferroelectric hysteresis measurements have been used for layer characterization.

Keywords: Films; Grain boundaries; PZT; PLZT; Ferroelectric properties

1. Introduction

Pulsed laser deposition (PLD) is an attractive technique for thin films growth. It consists in material removal by bombarding the surface of a target with short energetic pulses of a focussed laser beam of proper wavelength (laser ablation). Due to the high power density of the beam, plasma having a plume shape perpendicular to the target surface is generated at the incident point. The plasma contains ions of the target and of the gas atmosphere. The substrate to be coated is placed a few centimetres away from the target facing the top of the plasma plume. The condensation of the particles ejected from the target produces the growth of a thin film on the substrate surface. The possibility of transferring complicated stoichiometries directly from the target to a collector situated at a certain distance and position with respect to the target pushed this method to the top position, starting with the discovery of high temperature superconductors, in the late 1980s. Different classes of materials, including metals, semiconductors, and dielectrics were successfully deposited by PLD in vacuum or in various inert or chemically active atmospheres.[1,2] Ferroelectrics are a class of materials intensively studied in the form of thin films. They are characterized by a spontaneous polarization, which can be switched by applying an electric field.[3] This class of materials is very much investigated nowadays because of the large range of applications. Ferroelectrics can be used as capacitors, sensors and actuators, MEMS, optoelectronic devices, ferroelectric nonvolatile random access memories (FERAM), etc.[3,4]

Relaxor ferroelectric materials have a high dielectric constant and a broadened dielectric maximum compared to the normal ferroelectrics.[5] These properties make this kind of material suitable for dielectric, piezoelectric and electrostrictive applications.[6,7] $Pb(Mg_{1/3}Nb_{2/3})O_3$ (PMN) is the most known and studied relaxor ferroelectric, which exhibits high dielectric constant, with a maximum value of 15,000 at −15 °C, high electrostrictive coefficient and diffuse phase transition around −15 °C. For increasing the Curie temperature, a new material was synthesized, namely a combination of $Pb(Mg_{1/3}Nb_{2/3})O_3$ and $PbTiO_3$ (PT). PT is a highly anisotropic ferroelectric with large tetragonal distortion and a typical ferro–paraelectric transition at $T_c = 490$ °C, and with long range spontaneous ferroelectric order occurring below T_c.[3,5] The solid solutions between PMN and PT tend to combine properties from relaxor PMN

* Corresponding author. Tel.: +40 21 457 4470; fax: +40 21 457 4243.
E-mail address: dinescum@ifin.nipne.ro (M. Dinescu).

0955-2219/$ – see front matter © 2006 Elsevier Ltd. All rights reserved.
doi:10.1016/j.jeurceramsoc.2006.02.027

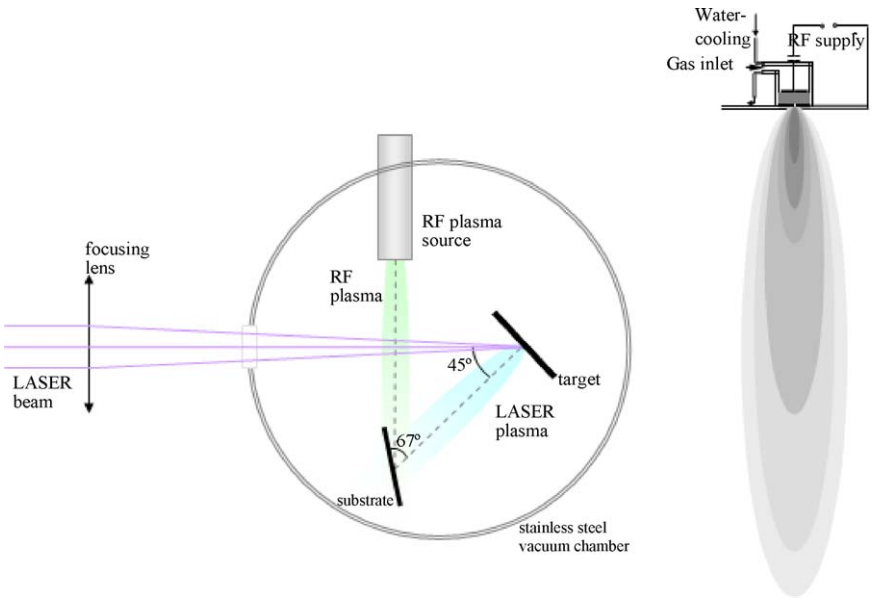

Fig. 1. Experimental set-up: (a) RF beam assisted PLD general system; (b) RF beam generation.

and ferroelectric PT. Single crystals of PMN–PT have been reported to exhibit extremely large piezoelectric strain (>1%) and a very high electromechanical coupling factor ($k_{33} > 90\%$). For small PT amounts, the composition presents large electrostrictive strain, and for about 35% PT, the PMN–PT system, near the phase boundary (MPB), presents significant piezoelectric effects.[5]

Lead titanate zirconate (PZT) materials are used both in bulk and as thin films, due to their interest for applications in piezoelectric transducers, ferroelectric memories, electrooptical devices, etc.[3,8] The variation of Zr/Ti ratio allows the structure modification from orthorhombic to rhombohedral and tetragonal and the modification of the physical properties.[3] Moreover, the doping with impurities like La or Nb can introduce big changes in their proprieties. For example, La substitution allows the gradual change in the material from ferroelectric to relaxor.

A review of our most important results concerning PLD and radiofrequency beam assisted PLD of thin films of the above-mentioned materials are discussed in this paper.

2. Experimental set-up

In Fig. 1 the deposition system for PLD and RF-PLD is presented. The beam from a Surelite II Nd:YAG laser was focused through a spherical lens on the target at 45° incidence. The pulsed laser can work at four wavelengths: 1064 nm (infrared radiation), 532 nm (green), 355 and 266 nm (ultraviolet radiation); the pulse duration is 5–7 ns and the repetition rate can be varied between 1 and 10 Hz. Ceramic pellets of PMN–PT with different PT compositions and of La- and Nb-modified PZT were used as targets.[4,6,7,9,10]

The laser fluence, oxygen pressure, and substrate temperature were varied in order to achieve the best deposition configuration. The films were deposited on different substrates: Si, Pt-coated Si, MgO, LSCO-coated MgO.

The difference from a classical PLD system is the presence of the RF discharge produced by a CESAR 1310RF generator working at 13.56 MHz and a maximum power of 1000 W. The discharge is generated in flowing oxygen between two parallel electrodes (16 mm diameter). It expands into the ablation chamber as a plasma beam through an aperture (~2 mm diameter) formed in the bottom electrode, which acts as a nozzle. The enhanced reactivity at the substrate surface between the ablated species and the ionized and excited species coming from the plasma beam may lead to improved characteristics of the deposited films, e.g. to prevent oxygen vacancies at the electrode-film interface and oxygen deficiency in the films. The deposition temperature may be also reduced because the RF discharge supplies additional energy, so the structures can be easily integrated in Si technology.

Thin films have been deposited starting from PMN–*x*PT targets, with different PT compositions (0, 10 and 20%).

Different target compositions were used for La-doped PZT: $Pb_{1-x}La_x(Zr_{0.65}Ti_{0.35})_{1-x/4}\square_{x/4}O_3$, $x = 0.02$ (PLZT-B 2/65/35); $Pb_{1-x}La_x(Zr_{0.65}Ti_{0.35})_{1-x/4}\square_{x/4}O_3$, $x = 0.09$ (PLZT-B 9/65/35), $Pb_{1-3x/2}La_x\square_{x/2}(Zr_{0.2}Ti_{0.8})O_3$, $x = 0.22$ (PLZT-A 22/20/80) and $Pb_{0.988}\square_{0.012}(Zr_{0.52}Ti_{0.48})_{0.976}Nb_{0.024}O_3$ (PZTN 52/48). The symbol □ indicates the vacancies.

For PLZT-B 2/65/35, La^{3+} ions substitute Pb^{2+} in the A sites of the perovskite lattice. According to this stoichiometry, the charge compensation is ensured by the formation of B-site vacancies (one B-site vacancy for four La^{3+} substituted ions). From these targets a set of films has been deposited on Pt/Si substrates by RF-assisted PLD in the following optimized conditions: target–substrate distance 5 cm, oxygen pressure 0.6 mbar, substrate temperature 650 °C, laser fluence 5 J/cm^2, laser wavelength 355 nm, RF power 100 W.

PZT 65/35 is rhombohedral, but the substitution of La^{3+} gradually decreases the distortion up to the formation of a cubic lattice for $x = 0.09$. From ferroelectric it becomes

Table 1
The deposition conditions for PMN-PT films[3]

Sample	Laser wavelengths (nm)	Reactive (oxygen) pressure (mbar)	Substrate temperature (°C)	Buffer layer (electrode)/substrate	ϕ_{laser} (J/cm^2)
PMN	1064	0.2	500	Au/Pt/NiCr/Al_2O_3	25
PMN	1064	0.2	400	Pt/Si	25
PMN–10%PT	266	0.4	500–600	LSCO/MgO	2
PMN–10%PT	266	0.4	500–600	LSCO/Si	2
PMN–10%PT	266	0.4	500–600	LSCO/Pt/Ti/MgO	2
PMN–10%PT	355	0.1	600	Pt/Ti/SiO_2/Si	3
PMN–10%PT	355	0.1	650	Pt/Ti/SiO_2/Si	3
PMN–10%PT	355	0.1	700	Pt/Ti/SiO_2/Si	3
PMN–10%PT	532	0.4	500–600	LSCO/Si	2
PMN–10%PT	532	0.4	500–600	Pt/Ti/Si	2
PMN–10%PT	1064	0.2	400	Pt/Ti/Si	25
PMN–10%PT	1064	0.4	600	LSCO/Si	2
PMN–10%PT	1064	0.6	500	LSCO/Si	25
PMN–20%PT	1064	0.2	400	Au/Pt/NiCr/Al_2O_3	25

relaxor with nanodomains instead of normal ferroelectric domains. Films have been deposited on Pt/Si substrates in the following optimized conditions: target–substrate distance 4 cm, oxygen pressure 0.3 mbar, substrate temperature 600 °C, laser fluence 3 J/cm^2, laser wavelength 355 nm, RF power 100 W.[9,10]

For PLZT-A 22/20/80, La^{3+} ions are substituted for Pb^{2+} in the A site of the perovskite structure with charge compensation given by the formation of A-site vacancies (one vacancy for each two La atoms). The introduction of La gradually decreases the tetragonality up to a cubic lattice for $x = 0.22$. This has been confirmed by XRD analysis of the target. Samples with this composition are relaxors. Films with this composition have been deposited on Pt/Si substrates in the following optimized conditions: target–substrate distance 5.3 cm, oxygen pressure 0.4 mbar, substrate temperature 650 °C, laser fluence 2 J/cm^2, laser wavelength 266 nm, RF power 200 W.[10–12]

For PZTN 52/48, Nb^{5+} enters in the B-site position substituting for Zr^{4+} (or Ti^{4+}) ions. Charge compensation is ensured by the formation of A-site vacancies (each pair of Nb ions produce one lead vacancy). Films have been deposited on Pt/Si substrates in the following optimized conditions: target–substrate distance 5 cm, oxygen pressure 0.4 mbar, substrate temperature 650 °C, laser fluence 2 J/cm^2, laser wavelength 266 nm, RF power 200 W.

Compositional, structural and morphological investigations of the deposited films have been performed by secondary ion mass spectrometry (SIMS), X-ray diffraction (XRD), scanning electron microscopy (SEM), transmission electron microscopy (TEM) and atomic force microscopy (AFM). Metallic Au/Cr top electrodes with diameters of 0.5–3 mm have been deposited by thermal evaporation for electrical measurements. Ferroelectric hysteresis loops have been obtained using a Radiant Technologies RT66A device in the automatic virtual ground mode, at different temperatures. Dielectric measurements have been performed as a function of frequency, AC driving field intensity and temperature using a HP4194A impedance analyzer and a Delta Design 9023 test chamber working at temperatures between 300 and −50 °C.

3. Results and discussions

3.1. PMN and PMN–PT thin films deposition

The conditions for PMN–PT thin films deposition are presented in Table 1. Structural investigations have shown that the best results have been obtained for films deposited on LSCO electrodes, which have been grown by PLD on Si substrates in the same experimental set-up as the PMN–PT thin films (Fig. 2a–c). It has been previously observed that perovskite oxide LSCO electrodes, in addition to their high electrical conductivity and good lattice matching with PMN–PT, are good buffer layers and prevent oxygen vacancies at the interface.[13] Our experimental results have also shown that the laser wavelengths and substrate-buffer layer-electrode combination strongly influence the structural properties of the films. Better properties have been obtained for films deposited using ultraviolet radiation. In order to increase the deposition efficiency we have also used high laser fluence in the infrared region, but in this case, in addition to a rougher surface morphology, a pyrochlore phase is obtained (Fig. 2d). This is probably due to modification of the target composition at the surface during ablation with the high-energy infrared laser beam. All films were crystalline and randomly oriented.[4]

SIMS analysis of selected samples revealed a small amount of interdiffusion between the PMN–PT film, the substrate and the buffer layer, and a uniform distribution of elements, especially for the PMN–PT film. The sharp interface was also confirmed by cross-section transmission electron microscopy analysis. A cross-sectional TEM image of a PMN film deposited on LSCO/Si is presented in Fig. 3. It can be observed that the PMN film growth was quasi-columnar: this is probably due to the columnar growth of LSCO film and to the small misfit between the two lattice parameters.[4]

AFM studies revealed rather smooth surfaces. The AFM image in Fig. 4 shows a typical image taken from the surface of a PMN film deposited on LSCO/Si at $pO_2 = 0.4$ mbar, laser fluence of 2 J/cm^2, $T = 600$ °C and a laser wavelength of 266 nm. The

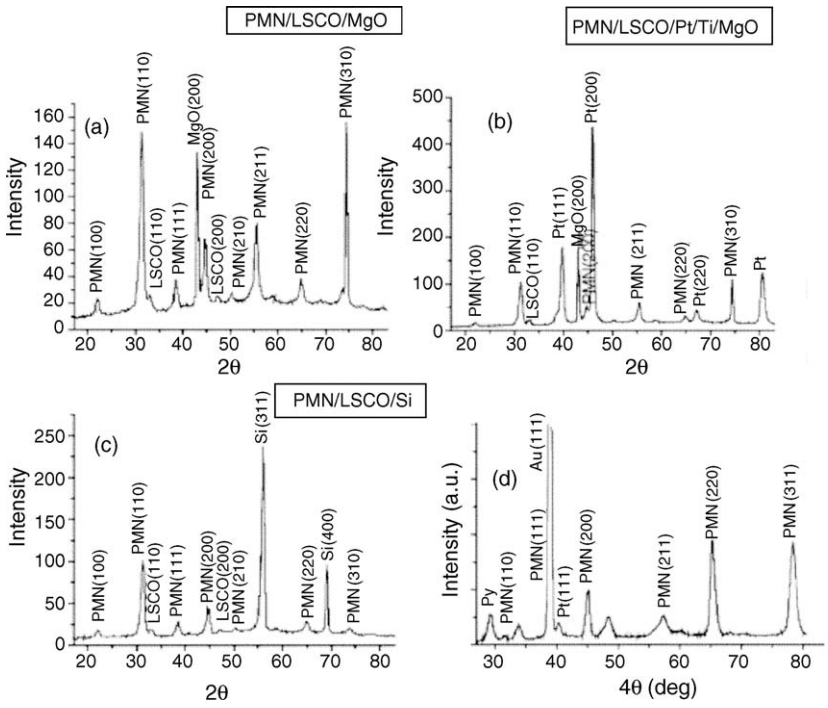

Fig. 2. X-ray diffraction spectra of PMN–10%PT films deposited at $pO_2 = 0.4$ mbar, laser fluence of 2 J/cm^2, $T = 600\,^{\circ}$C, $\lambda = 266$ nm: (a) LSCO/MgO; (b) Pt/Ti/MgO; (c) LSCO/Si; (d) PMN film deposited at $pO_2 = 0.2$ mbar, laser fluence of 25 J/cm^2, $T = 500\,^{\circ}$C, $\lambda = 1064$ nm, on Au/Pt/NiCr/Al_2O_3.[3]

height scale is 250 nm and the film has a roughness of approximately 11 nm.

The dielectric permittivity of PMN samples showed a broad maximum of the dielectric constant at the temperature T_m of approximately 0 °C (T_m is about −5 °C for bulk samples used as targets). The maximum relative dielectric constant was approximately 4000. The highest values of the real part of the dielectric constant at T_m have been obtained for PMN–10%PT films (approx. 4500). Room temperature values are shown in Table 2. The small dielectric constant values can be explained by the presence of a very thin interface layer between the PMN–PT and the electrode layers, with modified properties.[4]

All samples show a slim ferroelectric hysteresis loop (with a remanent polarization of approx. 1 μC/cm^2 and a coercive field of approx. 50 kV/cm) at ambient temperature (above T_m) as typically found for relaxors. The remanent polarization was increased at temperatures below T_m (approx. 11 μC/cm^2 at −10 °C). A piezoelectric response ($d_{33} = 40$–60 pm/V) was measured at ambient temperature on all types of samples, showing the existence of intrinsic polarization.[4]

3.2. PZT-based thin film deposition

XRD analysis shows that all deposited layers were polycrystalline and randomly oriented. PLZT-B 9/65/35 films present

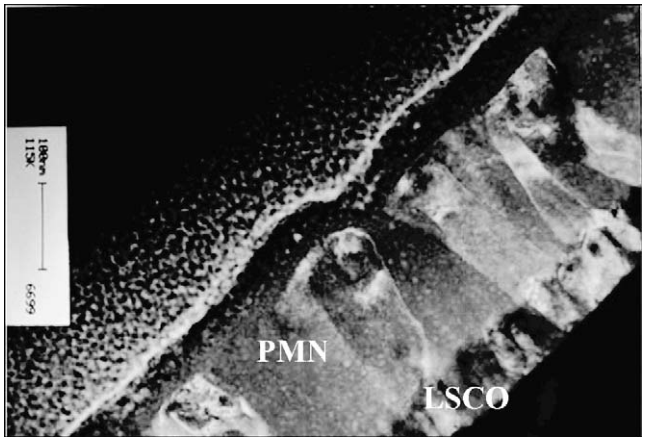

Fig. 3. Cross-section transmission electron microscopy image of a PMN/LSCO/Si heterostructure deposited at $pO_2 = 0.4$ mbar, laser fluence of 2 J/cm^2, $T = 600\,^{\circ}$C, $\lambda = 266$ nm.[3]

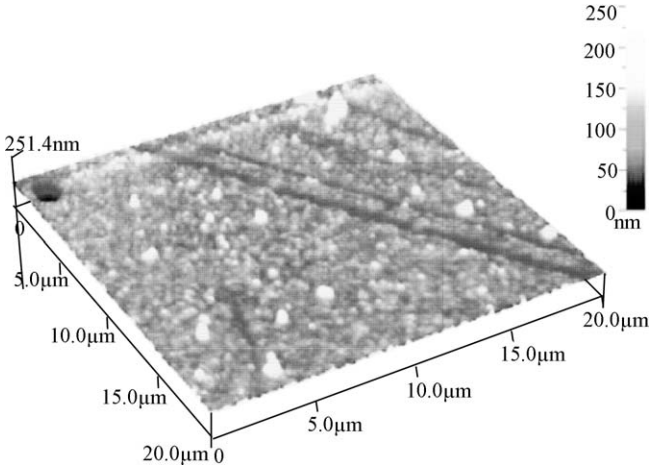

Fig. 4. Atomic force microscopy image of a PMN film surface for a layer deposited on LSCO/Si at $pO_2 = 0.4$ mbar, laser fluence of 2 J/cm^2, $T = 600\,^{\circ}$C, $\lambda = 266$ nm.[3]

Table 2
Dielectric properties of PMN–PT thin films at ambient temperature[3]

Sample	Buffer layer (electrode)/substrate	Dielectric constant (at 25 °C)	Resistivity (Ω cm)
PMN	Au/Pt/NiCr/Al_2O_3	880	10^{11}
PMN	Pt/Si	500	10^{12}
PMN–10%PT	LSCO/Si	250	10^{9}
PMN–10%PT	Pt/Ti/SiO_2/Si	470	10^{9}
PMN–20%PT	Au/Pt/NiCr/Al_2O_3	730	10^{9}

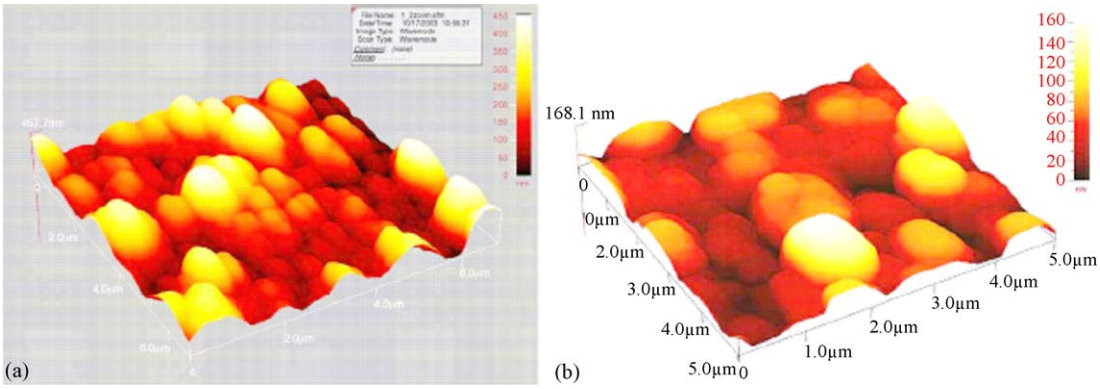

Fig. 5. AFM 3D images (a) 6 μm × 6 μm on PZTN 52/48 and (b) 5 μm × 5 μm on PLZT-B 9/65/35 films (film of about 500 nm thickness).[8]

a slight (1 1 0) preferred orientation. The obtained films were almost pure phase with some small amount of pyrochlore. AFM images show similar morphology for PLZT-B 2/65/35, PLZT-B 9/65/35 and PZTN 52/48 films, with uniform platelet-like grains with dimensions 500–800 nm (Fig. 5).[8] Films produced from PLZT-A 22/20/80 targets showed much smaller grains (100–200 nm) (Fig. 6).[8] The AFM-3D images presented in Fig. 5 were taken on (a) 6 μm × 6 μm on PZTN 52/48 and (b) 5 μm × 5 μm on PLZT-B 9/65/35 samples, while the image in Fig. 6 shows a 10 μm × 10 μm surface of PLZT-A sample.

In Fig. 7 is shown the variation of capacitance C as a function of frequency f for PLZT-A 22/20/80 films, for different values of the AC driving field E, up to 20 kV/cm. A similar dependence on frequency was registered also for the other samples.

The coercive field, determined from ferroelectric hysteresis loops, is above 50 kV/cm for all the ferroelectric films and above 30 kV/cm for the relaxor films, thus the AC field amplitude is in the sub-switching regime. Therefore, the employed phenomena correspond only to movements of normal domain walls (in ferroelectric PLZT-B 2/65/35 and PZTN 52/48 films) and nanodomain walls (in relaxor PLZT-B 9/65/35 and PLZT-A 22/20/80 films). It can be observed that the capacitance follows the relation $C(f, E) = C_0(E) - |a|/\ln(f)$, where C_0 is the static capacitance and a is a constant, dependent on temperature and sample properties. The linear decrease of the capacitance with log frequency can be ascribed to a domain wall pinning phe-

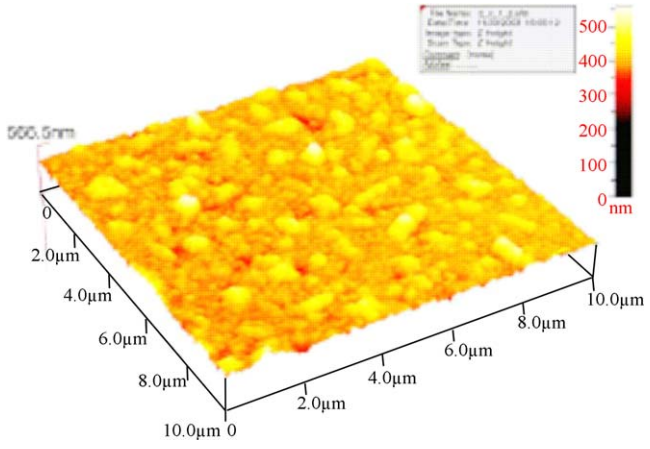

Fig. 6. AFM 3D image (10 μm × 10 μm) on a PLZT-A 22/20/80 (film of about 500 nm thickness).[8]

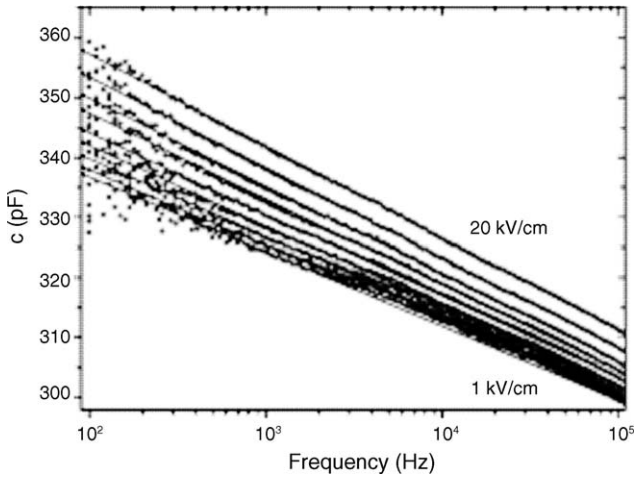

Fig. 7. Capacitance vs. frequency for different ac electric field amplitudes measured on a PLZT-A 22/20/80 (film of about 500 nm thickness). The amplitude of the driving field for the different displayed curves from bottom to top is: 1–4, 6, 8, 10, 12, 14, 16, 18 and 20 kV/cm.[8]

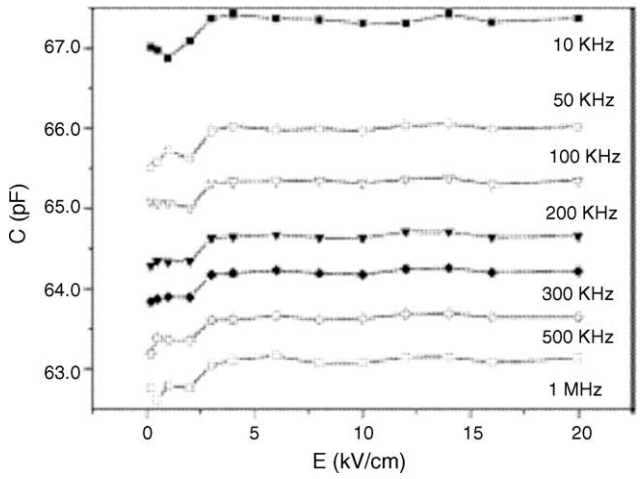

Fig. 8. Capacitance vs. driving field amplitude for a PLZT-B 9/65/35 film.[8]

nomenon in ferroelectrics, due to interaction of pinning centers with moving interfaces.[14,15] This corresponds to more general phenomena also found in magnetic materials and other systems.[16]

When plotted as a function of the ac field amplitude the capacitance of the investigated samples shows very different behaviour. Fig. 8 [10] presents results obtained for PLZT-B 9/65/35 samples for different frequency values up to 1 MHz. Similar behaviour but with different capacitance values was found for the PLZT-B 2/65/35 sample. Fig. 9 shows the same curves for PLZT-A 22/20/80; a similar behaviour is found for PZTN films. As observed in Fig. 8, the capacitance of PLZT-B 9/65/35 (and PLZT-B 2/65/35) films exhibits almost no variation with ac field amplitude up to 20 kV/cm, except for a small "threshold" at about 2.5 kV/cm. The capacitance of PLZT-A 22/20/80 (and PZTN 52/48) films have instead a nonlinear variation with E, as can be observed in Fig. 9. There are many differences in the chemical composition, crystal structure, morphology and domain configuration between the investigated films, but what is common to samples with C–E behaviors displayed in Figs. 8 and 9 is the vacancy types: PLZT-B 9/65/35 and PLZT-B 2/65/35 have B-site vacancies, while PLZT-A 22/20/80 and PZTN 52/48 have A-site vacancies. B-site vacancies are stronger pinning centers than A-site vacancies. The threshold in Fig. 8 could be due to a minimum energy value, which must be given to obtain the depinning of some domains. Further increase of the field amplitude up to 20 kV/cm does not alter the permittivity value. On the other side, A-site vacancies facilitate domain boundary motion and stress relief, so that small electric fields can displace domain walls. This could explain the high nonlinearity in the ac field behaviour of PLZT-A and PZTN samples.[10]

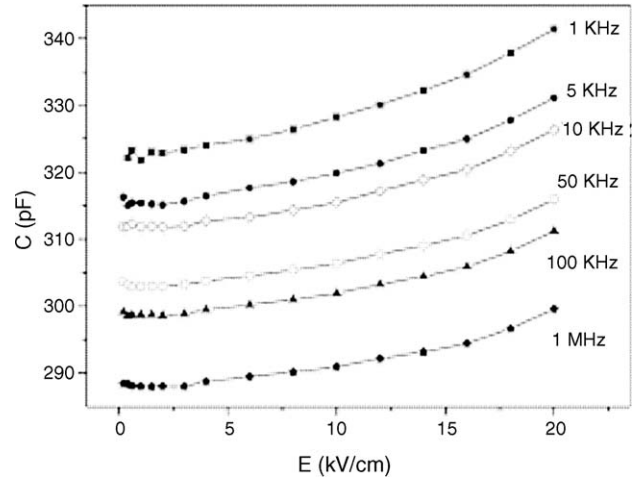

Fig. 9. Capacitance vs. driving field amplitude for a PLZT-A 22/20/80 film.[8]

4. Conclusions

PLD and radiofrequency beam-assisted PLD were demonstrated to be effective for obtaining crystalline, stoichiometric PMN–PT, La- and Nb-doped PZT films on different substrates without post-deposition annealing.

Even if there is interest in replacing the lead-based materials in a large variety of areas like food industry, environmental monitoring, health care and biomedical diagnosis with lead-free compounds like $LaTaO_3$, $Sr_xBa_{1-x}Nb_2O_6$ or $(Na_{1/2}Bi_{1/2})TiO_3$–$BaTiO_3$ instead of PZT, the Pb-based oxides still remain the materials with most attractive ferroelectric and relaxor properties.

References

1. Chrisey, D. B. and Hubler, G. K., ed., *Pulsed Laser Deposition of Thin Films*. John Wiley & Sons, New York, 1994.
2. Bäuerle, D., *Laser Processing and Chemistry*. Springer, Berlin, Heidelberg, New York, 1996.
3. Xu, Y., *Ferroelectric Materials and Their Applications*. North-Holland, Amsterdam, 1991.
4. Scarisoreanu, N., Craciun, F., Dinescu, G., Verardi, P. and Dinescu, M., Lead-based ferroelectric compounds deposited by PLD. *Thin Solid Films*, 2004, **453–454**, 399–405.
5. Samara, G. A., The relaxational properties of compositionally disordered ABO_3 perovskites. *J. Phys.: Condens. Matter*, 2003, **15**, R367–R411.
6. Brodoceanu, D., Scarisoreanu, N. D., Filipescu, M., Epurescu, G. N., Matei, D. G., Verardi, P. *et al.*, *Pulsed LASER Deposition of Oxide Thin Films, PPLA*. World Scientific Publishing Co. Pte. Ltd, 2003, pp. 41–46.
7. Verardi, P., Craciun, F., Scarisoreanu, N., Dinescu, M., Grigoriu, C., Galassi, C. *et al.*, Ferroelectric relaxor thin films grown by pulsed laser deposition. *Ferroelectrics*, 2003, **293**, 189–199.
8. Craciun, F., Verardi, P. and Dinescu, M., Piezoelectric thin films: processing and properties. In *Handbook of Thin Film Materials, Ferroelectric and Dielectric Thin Films*, *Vol 3*, ed. H. S. Nalwa. Academic Press, 2002, pp. 231–308, and references therein.
9. Craciun, F., Dinescu, M., Verardi, P., Scarisoreanu, N., Galassi, C. and Piazza, D., Dielectric spectroscopy measurements of relaxor ferroelectric PLZT 9/65/35 thin films obtained by RF assisted PLD. *Ferroelectrics*, 2004, **302**, 313–318.
10. Verardi, P., Craciun, F., Dinescu, M., Scarisoreanu, N., Moldovan, A., Purice, A. *et al.*, Properties of La and Nb-modified PZT thin films grown by radiofrequency assisted pulsed laser deposition. *Mater. Sci. Eng. B*, 2005, **118**, 39–43.
11. Craciun, F., Dinescu, M., Verardi, P., Scarisoreanu, N., Moldovan, A., Purice, A. *et al.*, Processing and characterization of ferroelectric thin films obtained by pulsed laser deposition. *J. Eur. Ceram. Soc.*, 2005, **25**, 2299–2303.
12. Craciun, F., Dinescu, M., Verardi, P., Scarisoreanu, N., Moldovan, A., Purice, A. *et al.*, Structural and electrical characterization of PLZT 22/20/80 relaxor films obtained by PLD and RF-PLD. *Appl. Surf. Sci.*, 2005, **248**, 329–333.

13. Maria, J. P., Hackenberger, W. and Trolier-McKinstry, S., Phase development and electrical properties analysis of pulsed laser depositing $Pb(Mg_{1/3}Nb_{2/3})O_3$–$PbTiO_3$ (70/30) epitaxial thin films. *J. Appl. Phys.*, 1998, **84**, 5147–5154.
14. Taylor, D. V. and Damjanovic, D., Evidence of domain walls contribution to the dielectric permittivity in PZT thin films at sub-switching fields. *J. Appl. Phys.*, 1997, **82**, 1973–1975.
15. Damjanovic, D., Logarithmic frequency dependence of the piezoelectric effect due to pinning ferroelectric-ferroelastic domain walls. *Phys. Rev. B*, 1997, **55**, R649–R652.
16. Natterman, T., Shapir, Y. and Vilfan, I., Interface pinning and dynamics in random systems. *Phys. Rev. B*, 1990, **42**, 8577–8586.